Experimental realization of phase-conjugate optical coherence tomography

Julien Le Gouët, Dheera Venkatraman,* Franco N. C. Wong, and Jeffrey H. Shapiro

Research Laboratory of Electronics, Massachusetts Institute of Technology, Cambridge, Massachusetts 02139, USA
**Corresponding author: dheera@mit.edu*

Received November 10, 2009; revised January 7, 2010; accepted February 5, 2010;
posted February 25, 2010 (Doc. ID 119815); published March 26, 2010

We demonstrate phase-conjugate optical coherence tomography (PC-OCT) using a classical source of phase-sensitive cross-correlated beams to achieve measurement improvements shared by quantum OCT (Q-OCT): a factor-of-2 enhancement in axial resolution and even-order dispersion cancellation. Compared with coincidence counting used in Q-OCT, PC-OCT employs standard photodetection that results in much faster data acquisitions. This work belongs to a new class of classical techniques inspired by quantum methods that have advantages once thought to be exclusively quantum mechanical. © 2010 Optical Society of America

OCIS codes: 180.1655, 110.4500, 190.4410, 190.5040, 270.0270.

Quantum resources have yielded many interesting effects, such as Hong–Ou–Mandel (HOM) interference [1] and dispersion cancellation [2,3], that have been thought to be intrinsically nonclassical. One example is quantum-optical coherence tomography (Q-OCT), which was proposed by Abouraddy *et al.* [4] and later demonstrated by Nasr *et al.* [5]. It uses entangled photon pairs and HOM interferometry to achieve 2× improvement in axial resolution with even-order dispersion cancellation in comparison with classical OCT. Recently, Resch *et al.* used classical chirped pulses or frequency correlated pulses to obtain the same HOM interference signature [6] and dispersion cancellation [7] with much higher signal-to-noise ratios. Even the features of Q-OCT have been reproduced with classical chirped-pulse interferometry [8], in agreement with Erkmen and Shapiro's analysis, which argues that Q-OCT's measurement characteristics are not inherently quantum [9].

Erkmen and Shapiro proposed another technique, called phase-conjugate OCT (PC-OCT), to reap Q-OCT's advantages without its slow acquisition speed [9]. PC-OCT uses classical signal and reference beams with phase-sensitive cross correlation. The signal interrogates the sample, and the output light is amplified, phase conjugated, and sent back to the sample for a second interrogation. The return phase-conjugate signal is recombined with the reference beam for interference measurement using a standard photodetector. The double-pass configuration yields a 2× axial resolution improvement, and the phase conjugation provides spectral phase reversal that compensates for even-order dispersion in the propagation medium. Losses due to the double-pass configuration can be compensated by the amplifier. We report here a proof-of-principle experiment of PC-OCT, showing that it achieves the key benefits as Q-OCT with a much higher acquisition speed.

PC-OCT requires two key components: a broadband source of phase-sensitive cross-correlated signal and reference beams, and a broadband phase conjugator. Broad bandwidth is desirable, because bandwidth sets the axial resolution of an OCT measurement. We have recently developed these tools in strongly pumped parametric fluorescence for the former and parametric amplification for the latter [10]. Using a mode-locked pump laser at 780 nm with an average power of 2 W, we produced amplified spontaneous parametric downconversion (SPDC) in a 20 mm periodically poled MgO-doped lithium niobate (PP-MgO:LN) crystal with a spectral bandwidth of over 100 nm centered at 1560 nm. With 1.9 W of pump power, we measured a single-mode fiber-coupled fluorescence spectral brightness of 1 nW/nm. For our operating bandwidth of ~6 nm, the signal output contained ~760 photons per pulse, much higher than the flux (<1 pair/pulse) of weakly pumped SPDC sources typically used for biphoton generation [1,2,5].

We also used a broadband optical parametric amplifier (OPA) to provide a gain of nearly 20 dB with the spectral phase reversal needed for PC-OCT [10]. For an input pulse that has been broadened by a dispersive medium, the OPA reverses the chirp in the phase-conjugate output pulse. As a result, after propagation through the same dispersive medium, the broadening in the phase-conjugate pulse is undone, and the pulse reverts to its original input shape.

Figure 1 shows the PC-OCT experimental setup. We coupled the broadband amplified SPDC output into a single-mode, fiber-coupled, coarse, wavelength division multiplexer (CWDM1) to create separate sig-

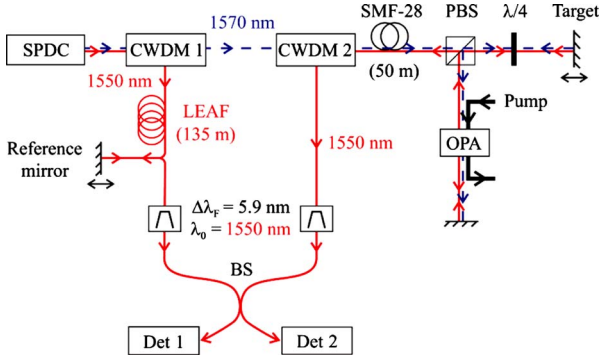

Fig. 1. (Color online) PC-OCT experimental setup. PBS, polarizing beam splitter; BS, 50:50 fiber beam splitter.

nal and reference beams in 16-nm-wide channels centered at ~1570 and ~1550 nm, respectively. The 1570 nm signal channel was routed to the sample through CWDM2 and a 50-m-long SMF-28 fiber that served to simulate sample dispersion. A circulator composed of a free-space polarizing beam splitter (PBS) and a quarter-wave plate simplified the double-pass configuration. In the first pass, the signal interrogated the sample, and the reflected signal was sent to the OPA to generate the amplified phase-conjugate beam. The 1550 nm phase conjugated signal was retroreflected to interrogate the sample a second time, coupled back into the long SMF-28 fiber, and then routed by CWDM2 to the interferometer.

The 1550 nm reference beam was passed through a dispersion-shifted fiber (LEAF) whose 135 m length was selected to match the total signal path length. We chose the LEAF fiber to reduce dispersion in the reference channel so that we could evaluate the PC-OCT setup's signal-path dispersion. A high-reflectivity mirror was mounted on a piezoelectric transducer (PZT) for quick scan of the reference path length (at 80 Hz). In addition, the entire PZT mirror was on a motorized translation stage that served as an adjustable free-space reference delay line. Before the 50:50 fiber beam splitter, a free-space interference filter centered at $\lambda_0 = 1550$ nm with an FWHM $\Delta\lambda_F = 5.9 \pm 0.2$ nm was added in each channel to control the spectral bandwidth and hence the axial resolution.

Typically, 2.5 nW of power was applied to each arm of the interferometer, whose outputs were measured with a high-sensitivity (0.1 pW) HP8163A InGaAs power meter. From the normalized difference between the two outputs, we removed the effects of source power fluctuations. At each position of the reference delay line, we used the PZT to scan the reference path length over more than one interference fringe. We obtained the amplitude of the interference envelope from the maximum and minimum recorded values as a function of the delay-line position. The expected width of the envelope is the same as in classical OCT for a given spectral width. However, owing to the double interrogation of the sample, the signal delay is twice as big. Therefore, for a given positional change Δz_S of the sample, we expect a reference delay shift $\Delta z_R = 2\Delta z_S$, hence the 2× axial resolution enhancement. In other words, identical reference delays in classical and phase-conjugate OCT allow one to resolve a layer half as thick in the latter. The duration of an envelope scan, of less than 3 min, was limited by the low speed of the motorized translation stage (~100 μm/s).

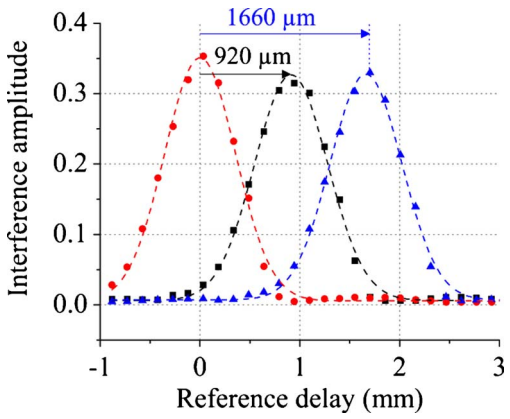

Fig. 2. (Color online) PC-OCT interference envelopes measured at three positions of the target mirror with a relative separation of 450 μm. Envelope widths (FWHM) are 890 μm, in excellent agreement with the dispersion cancellation model.

Figure 2 shows successive scans of the interference envelope amplitudes at three positions of a high-reflectivity target mirror with a relative separation of $\Delta z_S = 450$ μm. Averaging several envelopes like those in Fig. 2 yields an interference envelope width (FWHM) $L_{\mathrm{OCT}} = 890 \pm 30$ μm. The measured reference delay shift was 920 ± 20 μm (1660 ± 20 μm) between the peaks of the left and middle (right) curves. The measured values are in line with the expected $\Delta z_R = 2\Delta z_S$ behavior of PC-OCT, thus demonstrating its 2× axial resolution improvement. For the right curve, the ~7% discrepancy was caused by the effect of room temperature fluctuations on the effective fiber lengths. A separate temperature monitor showed temperature variation of ±0.75°C in 10 min cycles, with a corresponding PC-OCT measurement variance of ~200 μm, suggesting that improvements would be needed for small target shifts. This could be done by better temperature control of the reference arm, or by faster acquisitions. Note that this effect was noticeable only because we added long fibers to produce a known amount of dispersion.

The PC-OCT resolution is given by the coherence length of the signal and reference pulses. Assuming no dispersive components, the FWHM length of the signal and reference intensity pulses is determined by the spectral filter's Gaussian FWHM bandwidth, $L_0 = 0.44\lambda_0^2/\Delta\lambda_F = 179 \pm 6$ μm. A dispersive medium of length z broadens a Gaussian pulse according to $L(z)^2 = L_0^2 + (c\Delta\lambda_F D z)^2$, where D is the dispersion coefficient of the medium. The interference envelope is given by the convolution between the conjugate signal (S) and reference (R) fields with a width (FWHM)

$$L_{\mathrm{OCT}}^2 = 4L_0^2 + (c\Delta\lambda_F)^2(D_S z_{S1} - D_S z_{S2} + D_R z_R)^2, \quad (1)$$

where we allow the fiber lengths for the signal (z_{S1}) and conjugate signal (z_{S2}) to be different. Dispersion cancellation in PC-OCT is manifested in the opposite sign of the signal and conjugate signal contributions.

The SMF-28 fiber length from the amplified SPDC to the target was 77.1 m (z_{S1}), and 71.2 m (z_{S2}) from the target to the fiber beam splitter. As a result, there was a net fiber length of 5.9 m in which dispersion was not cancelled. The dispersion coefficient of the SMF-28 fiber D_{SMF} is taken as 17 ps/nm/km in the 1550–1570 nm range. To match the time delay in the signal arm, we added 135 m (z_{R1}) of LEAF fiber ($D_{\mathrm{LEAF}} = 4.2$ ps/nm/km at 1550 nm) to the reference arm, in addition to 18.9 m (z_{R2}) of SMF-28 fiber already in the setup, leading to $D_R z_R = D_{\mathrm{LEAF}} z_{R1} + D_{\mathrm{SMF}} z_{R2}$ in Eq. (1). Finally, we note that the reference mirror change is half of the actual change in the

reference delay line. We obtain an FWHM PC-OCT envelope width $L_{OCT}=893\pm30$ μm, which is in excellent agreement with the measured value of 890 ± 30 μm. Without dispersion cancellation, the pulse broadening in the signal arm would have led to a PC-OCT envelope width of 3.02 mm, or more than three times our measured value, clearly indicating that dispersion cancellation was achieved in the signal path.

The PC-OCT technique can also be applied to detecting weakly reflecting interfaces. Figure 3 shows the PC-OCT measurement of a partially reflecting household mirror with an aluminum backing. The glass had a thickness $d=1.74\pm0.01$ mm and a refractive index $n\approx1.5$. The origin of the peaks are peak 1, weak reflection at the air-glass interface; peak 2, main reflection at the glass-aluminum interface; and peak 3, weak reflection due to a double reflection inside the glass. The expected reference delays are thus $\Delta z_{1-2}=nd=2.61$ mm and $\Delta z_{1-3}=5.22$ mm, which are in very good agreement with the measurement results. The two weak inner peaks were also observed in the high reflector target measurements and were likely caused by a double reflection at an interface within the interference-filter cavity construction.

Because we used SPDC (in a strongly pumped regime), it might be tempting to attribute our results to the entangled nature of the signal and idler outputs or to potential squeezing between the two beams. While there might be quantum features in amplified SPDC that could be exploited, our operating regime and our detection method would not be capable of utilizing them. For example, the output contained hundreds of photons per pulse [10], so that its direct detection measurement statistics are best described classically. In addition, we used standard photodetection to measure the signal-reference interference, i.e.,

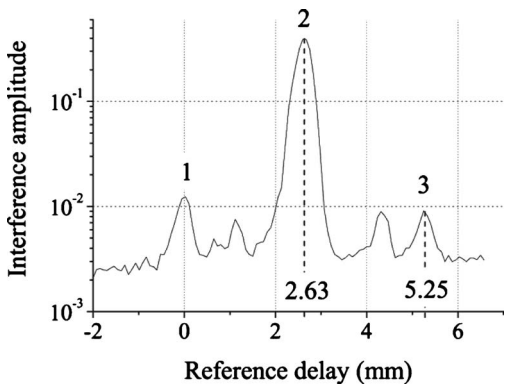

Fig. 3. Signature of PC-OCT measurement of a household mirror, made of a 1.74-mm-thick piece of glass with a thin aluminum coating on its back.

no single-photon coincidence counting or homodyne measurements were made. We should stress that amplified SPDC is used because it is the most convenient broadband source with the maximum classically allowable phase-sensitive cross correlations.

In summary, we have implemented PC-OCT using a classical source and standard photodetection to achieve fast acquisition times. Our proof-of-principle experiment verifies the two key PC-OCT benefits of $2\times$ axial resolution improvement and even-order dispersion cancellation in the sample path in comparison with classical OCT. Unlike Q-OCT, dispersion in the reference arm is not compensated in PC-OCT, which is usually not a significant issue, because the reference arm is local and in principle zero-dispersion fibers can be used. It is worth noting that the same double-pass configuration in PC-OCT could be applied to standard OCT to obtain the same resolution enhancement, but dispersive broadening in this case would be twice as severe. For PC-OCT dispersion cancellation to work in practical applications the round-trip transit times must be short compared with the fluctuations of the dispersion. Future improvements may include using a much broader SPDC bandwidth via chirped grating in periodically poled lithium niobate to achieve submicrometer PC-OCT resolution [11].

This work was supported by the Defense Advanced Research Projects Agency (DARPA) Quantum Sensors Program and the U.S. Army Research Office (USARO).

References

1. C. K. Hong, Z. Y. Ou, and L. Mandel, Phys. Rev. Lett. **59**, 2044 (1987).
2. A. M. Steinberg, P. G. Kwiat, and R. Y. Chiao, Phys. Rev. Lett. **68**, 2421 (1992).
3. J. D. Franson, Phys. Rev. A **45**, 3126 (1992).
4. A. F. Abouraddy, M. B. Nasr, B. E. A. Saleh, A. V. Sergienko, and M. C. Teich, Phys. Rev. A **65**, 053817 (2002).
5. M. B. Nasr, B. E. A. Saleh, A. V. Sergienko, and M. C. Teich, Phys. Rev. Lett. **91**, 083601 (2003).
6. R. Kaltenbaek, J. Lavoie, D. N. Biggerstaff, and K. J. Resch, Nat. Phys. **4**, 864 (2008).
7. K. J. Resch, P. Puvanathasan, J. S. Lundeen, M. W. Mitchell, and K. Bizheva, Opt. Express **15**, 8797 (2007).
8. J. Lavoie, R. Kaltenbaek, and K. J. Resch, Opt. Express **17**, 3818 (2009).
9. B. I. Erkmen and J. H. Shapiro, Phys. Rev. A **74**, 041601(R) (2006).
10. J. Le Gouët, D. Venkatraman, F. N. C. Wong, and J. H. Shapiro, Opt. Express **17**, 17874 (2009).
11. M. B. Nasr, O. Minaeva, G. N. Goltsman, A. V. Sergienko, B. E. A. Saleh, and M. C. Teich, Opt. Express **16**, 15104 (2008).